ACS Catalysis

Research Article

pubs.acs.org/acscatalysis

Silica-Supported Au−CuO_x Hybrid Nanocrystals as Active and Selective Catalysts for the Formation of Acetaldehyde from the Oxidation of Ethanol

J. Chris Bauer,[†] Gabriel M. Veith,[⊥] Lawrence F. Allard,[∥] Yatsandra Oyola,[†] Steve H. Overbury,[†,‡] and Sheng Dai*[,†,‡,§]

[†]Chemical Sciences Division, [⊥]Materials Sciences and Technology Division, Oak Ridge National Laboratory, Oak Ridge, Tennessee 37821, United States

[‡]Center for Nanophase Material Sciences, [∥]Physical Sciences Directorate, Oak Ridge National Laboratory, Oak Ridge, Tennessee 37831, United States

[§]Department of Chemistry, University of Tennessee, Knoxville, Tennessee 37996-1600, United States

ABSTRACT: The selective oxidation of ethanol with molecular O_2 is increasingly becoming an important process to develop fine chemicals because it can be obtained from renewable biomass feedstock while reducing the demand on fossil fuels. We have synthesized silica-supported Au−Cu alloy nanoparticles, and through an oxidative dealloying process, we have developed Au−CuO_x hybrid catalysts for the selective oxidation of ethanol into acetaldehyde. Using a combination of XRD, XPS, and HR-STEM experiments, we have confirmed that the active catalyst is a Au core with a thin CuO_x shell. Oxidation of the $AuCu/SiO_2$ alloy catalyst at 300 °C was found to produce the most active and stable catalyst for ethanol conversion (~90%) with the highest selectivity (~80−90%) at a reaction temperature of 200 °C for 50 h on-stream. TEM and XRD results show that Au−CuO_x/SiO_2 catalysts calcined at 300 and 500 °C are also more resistant to sintering during pretreatment and catalytic conditions than pure gold supported on silica. Furthermore, the silica-supported Au−CuO_x catalysts (calcined at 300 and 500 °C) were also found to be more active and selective in the dehydrogenation of ethanol to form acetaldehyde. It is likely that the increased interfacial contact between the Au and CuO_x forms the most active site on the catalyst and is responsible for the enhanced catalytic properties when compared with pure Au/SiO_2.

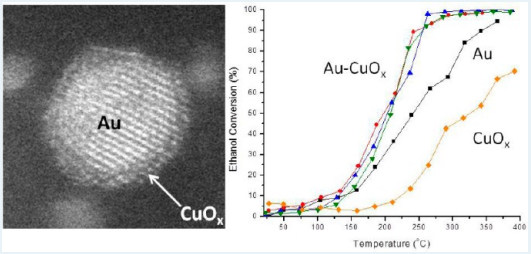

KEYWORDS: *Au catalysis, AuCu alloy, ethanol oxidation, acetaldehyde, dehydrogenation, heterostructure*

INTRODUCTION

The selective oxidation of biomass-derived ethanol to produce fine and specialty chemicals, such as acetaldehyde, ethylene, butadiene, acetic acid, etc., may potentially become an important process in the chemical industry.[1,2] Bioethanol is already in production around the world, and its availability is expected to increase in the next few years which may help to reduce the demand on fossil fuels as a feedstock.[1] It is also derived from biomass feed stock, which is a renewable resource. Furthermore, the selective oxidation of ethanol, as well as other alcohols, has increasingly become important as an alternative pathway to produce fine chemicals.[3] Unfortunately, the use of toxic and expensive[4] oxidants, such as oxygenates, permanganates, and peroxides, often provides poor selectivity and requires extra separation and waste treatment steps. To avoid potential ecological contamination from inorganic oxidizers, an intense research effort has focused on the development of a solid catalyst capable of activating molecular O_2 as an inexpensive and clean oxidant.

Supported metal catalysts have emerged as very active catalysts for the oxidation of alcohols.[5] For example, palladium nanoparticles supported on hydroxypatite (HAP) have received a lot of attention because of the high turnover numbers for the oxidation of 1-phenylethanol at atmospheric pressure in O_2 and is considered as the standard.[6] Pd and Pt nanoparticles have also been found to be highly active for aqueous-phase ethanol oxidation.[7] Unfortunately, these metals exhibit poor product selectivity because they require high reaction temperatures.

Prati and co-workers were among the first to report the use of heterogeneous gold catalyst supported on carbon to oxidize ethane-1,2-diol and propane-1,2-diol to glycolic and lactic acids using molecular oxygen.[8−10] They later discovered that medium-sized Au particles were the most active on carbon support, as opposed to the smaller particles showing more activity on oxide supports during the oxidation of ethylene glycol.[11] Biella demonstrated that Au/SiO_2 was capable of oxidizing a variety of primary and secondary aliphatic alcohols to aldehydes and ketones in the gas phase.[12] Hutchings reported on the oxidation of glycerol using Au, Pd, and Pt supported on carbon supports and found that Au could obtain 100% selectivity toward glyceric

Received: April 9, 2012
Revised: September 25, 2012
Published: October 18, 2012

acid with high conversion when elevated O_2 pressure and a base was used.[13] Under similar reaction conditions, Prati's group revealed that Au−Pt and Au−Pd particles not only increased the activity, but also could control the distribution of products.[14] Hutchings later found that supported Au and Au−Pd alloy nanoparticle catalysts were able to oxidize primary alcohols and benzyl alcohol with high activity and selectivity under solvent-free conditions using no base.[15−20]

Supported Au catalysts have been found to be active for the selective oxidation of ethanol into fine chemicals, such as acetaldehyde, ethylene, butadiene, acetic acid, and ethyl acetate.[21] Christensen found that Au supported on $MgAl_2O_3$ was not only active for the oxidation of aqueous solutions of ethanol, but it was also considerably more selective toward acetic acid formation as compared with the corresponding Pt and Pd catalysts.[22] It was concluded that the reaction pathway of the catalytic oxidation of ethanol proceeded through the oxygen-assisted dehydrogenation of ethanol to form acetaldehyde (rate-determining step) before forming acetic acid.[2] Furthermore, the selectivity toward acetic acid or ethyl acetate formation could be controlled by adjusting the ethanol concentration. The effect of the support on the Au-catalyzed oxidation of ethanol was examined, and the order of activity, as well as resistance to Au leaching, was reported as ZnO > TiO_2 > Al_2O_3.[23] A size effect of Au nanoparticles supported on SiO_2 revealed that a particle diameter of 5 nm formed the most active catalyst.[24] The catalytic activity of Au nanoparticles could also be increased through the addition of trace amounts of promoters, such as metal carbonates, acetate, and borates.[25]

The low-temperature alcohol oxidation reactions described thus far have dealt solely with solution-phase batch reactions that require elevated O_2 pressures, long reaction times, and catalyst separation steps. Gas-phase reactions do not require a solvent or catalyst separation, which makes them more attractive; however, higher temperatures are required, which results in a poorer selectivity of products. For instance, Stucky reported that 6.3 nm Au/SiO_2 showed more than 40% conversion with less than 80% yield of acetaldehyde at 200 °C.[26] This finding also agrees with Guan et al., who also concluded that a diameter of ∼6 nm for Au particles was the optimum size because of the surface steps with a suitable geometry to remove the β-H from the ethoxy species.[27] A combination of TPD and IR studies indicated that ethanol adsorbs strongly on the Au surface (when supported on SiO_2 or carbon) and can convert to different surface species.[28] When CeO_2 is used as a support, it is believed it cooperatively works with Au, and the reaction occurs at the interface. A similar observation was indirectly made when Au/TiO_2 showed low temperature ethanol conversion (∼60%) at ∼120 °C before reaching 100% conversion near 280 °C.[29] More inert supports, such as SiO_2 or Al_2O_3, did not show such behavior, and it was speculated that some sort of oxygen species on the Au−TiO_2 interface may be involved.

Recent advances in catalysis have shown that merging of metal or oxide phases (or both) into closely coupled hetero-structured nanoparticles (Janus particles, core−shell, etc.) can lead to altered catalytic activity, selectivity, and stability. For example, Wang et al. showed that the formation of Au−Fe_3O_4 "dumbbell" nanoparticles was more active for low-temperature CO oxidation than a commercial Au−FeO_x catalyst.[30] Okumura et al. discovered that when Ir was added to TiO_2, the catalytic activity improved at higher temperatures.[31] Further investigation through TEM observation and DFT calculations revealed that Au-capped IrO_2 pillars on TiO_2 was the active catalyst, which preserved the sintering resistance of Au.[32,33] In a different approach, Zhou et al. synthesized Au−Ni alloy nanoparticles supported on SiO_2 and found that oxidative treatment led to the formation of coupled Au−NiO heterostructures that were active and stable catalysts for CO oxidation.[34,35] Through XANES and EXAFS experiments it was reasoned that the Au particles were decorated with small NiO particles, and the interface between the two helped to enhance the overall catalytic properties. In a separate study, intermetallic AuSn nanoparticles were also found to be stable and active for CO oxidation after undergoing oxidative pretreatment to form Au−SnO_2.[36]

Recently, we studied the catalytic properties of Au−Cu alloy nanoparticles and determined that their most active form for the CO oxidation reaction was Au−CuO_x.[37] Through a combination of in situ XRD and XAS experiments, we were able to determine that the oxidative dealloying of Au−Cu began around 150 °C, and the dealloying process was completed by 300 °C to form a Au−CuO_x heterostructure. After calcination at 300 °C, complete CO conversion at room temperature could be obtained, and in conjunction with FTIR, it was concluded that when Cu is alloyed with Au, the catalyst is inactive. Similar findings were obtained by Liu et al., who additionally showed that the selective oxidation of CO in the presence of H_2 was improved with the Au−CuO_x catalyst.[38] Zhong et al. studied the activation and deactivation of a Au−Cu/SBA-15 catalyst and concluded that the most active phase was composed of Au and CuO particles.[39] Under PROX conditions, CuO particles were partially reduced to Cu_2O and when Au and Cu alloyed a drop in catalytic activity was observed.

In this work, we use the Au−Cu alloy as an example to demonstrate that an oxidative dealloying process to phase-separate the AuCu alloy into a Au−CuO_x heterostructure is a viable method to design more complex nanoparticle catalysts. The catalytic properties of the Au−CuO_x heterostructure were examined to study the catalytic affects on catalytic activity, selectivity, and stability for the oxidative dehydrogenation of ethanol. Silica was also chosen as a catalyst support because it is relatively inert[40] and nonreducible and, therefore, will have little influence on the catalytic activity of the AuCu alloy. Additional advantages silica can offer as a catalyst support are that it has a high surface area, thermal stability, and mechanical strength; however, the high pH required to hydrolyze $HAuCl_4{\cdot}3H_2O$ and the low isoelectric point of silica causes a weak interaction with Au, and traditional DP methods often result in large catalytically inactive particles. To overcome this problem, a modified DP method was used in which a cationic Au species ($Au(ethylenediamine)_2Cl_3$) strongly interacted with the negative SiO_2 surface at a high pH to form small, stable Au particles.

EXPERIMENTAL METHODS

Materials. All chemicals were used as received and purchased from Aldrich unless otherwise stated: copper(II) acetate, 98%; gold(III) chloride trihydrate, ACS reagent; 1-octadecene, tech, 90%; oleylamine, approximate C18 content 80−90%; oleic acid technical grade, 90%; ethylenediamine, Reagentplus, >99%; and fumed silica, 99.8%.

Synthesis of $Au(en)_2Cl_3$ (en = ethylenediamine). Au nanoparticles supported on silica were prepared by a previously reported procedure.[41] To synthesize the $Au(en)_2Cl_3$ precursor, ethylenediamine (0.45 mL) was slowly added to an aqueous solution of $HAuCl_4{\cdot}3H_2O$ (1.0 g in 10.0 mL of DI H_2O) to form a transparent brown solution. After stirring for 30 min, 70.0 mL of ethanol was added to induce precipitation.

dx.doi.org/10.1021/cs300551r | ACS Catal. 2012, 2, 2537−2546

The final product was centrifuged, washed in ethanol, and dried overnight.

Synthesis of Au/SiO_2 and CuO_x/SiO_2 Catalysts. According to our previously reported procedure,[41] 80 mg of $Au(en)_2Cl_3$ was dissolved in 100 mL of DI H_2O to make 3.6 wt % Au loading on silica. A 1.0 M solution of NaOH was added dropwise to raise the pH to 10.5. A 1.0 g portion of SiO_2 was added, and the pH rapidly decreased. Over the next 30 min, 1.0 M NaOH solution was added to maintain the pH at 10.5. The mixture was then transferred to a 60 °C water bath for 2 h. The final product was collected by centrifugation, washed in H_2O, dispersed by a vortexer and centrifuged four times. The yellowish product was dried in a vacuum oven for 5 h at 70 °C and reduced at 150 °C in 10% H_2/Ar for 1.0 h to obtain a red powder.

Cu/SiO_2 catalysts were synthesized through an impregnation method reported in the literature,[42] in which a calculated amount of $Cu(NO_3)_2$ was dissolved in DI H_2O (0.9 cm^3/g of SiO_2). The $Cu(NO_3)_2$ solution was brought to a pH of 11 by the addition of ammonium hydroxide. The silica was then added to the solution to obtain ~3 wt % Cu loading, and the solution was stirred at room temperature until the copper uptake reached equilibrium. The powder was collected by centrifugation and washed with DI water several times before being allowed to dry overnight in a vacuum oven at 100 °C. The catalyst was then reduced in 10% H_2 for 2 h at 400 °C and calcined at 300 °C in 10% O_2 at 300 °C to generate CuO_x/SiO_2.

Synthesis of $AuCu/SiO_2$ Catalyst. AuCu alloy nanoparticles supported on SiO_2 were prepared by first dissolving $Cu(C_2H_3O_2)_2$ (0.0501 mmol) into 1-octadecene (20 mL), oleic acid (1.683 mmol), and oleylamine (1.683 mmol) in a 100 mL, three-neck, round-bottom flask. Then Au/SiO_2 (180 mg, 3.6 wt % Au, and 0.0387 mmol of Au) was added to the solution, and the mixture was magnetically stirred under flowing Ar gas. The temperature was first raised to 120 °C for 20 min to remove water then increased to 305 °C for 1.5 h. The heating mantle was removed, and the reaction mixture was cooled to room temperature, diluted in ethanol, and centrifuged at 7500 rpm for 7 min. The final product was washed by suspending the powder in ethanol and centrifuging four times before drying in air. The silica-supported Au_3Cu and $AuCu_3$ were carried out under identical conditions except molar ratios of 0.5 and 4 of Cu/Au were used.

Characterization with XRD, TEM, and XPS. XRD data were collected at room temperature on a PANalytical X'Pert Pro MPD diffractometer over the range from 30 to 90° 2θ using an X'Celerator RTMS detector. TEM experiments were carried out on a Zeiss Libra 120 TEM operated at 120 kV. High-angle annular dark-field (HAADF) and bright-field images were acquired in scanning transmission mode (STEM) on a 200 kV JEOL 2200FS STEM/TEM instrument equipped with a CEOS GmbH (Heidelberg, Germany) hexapole aberration corrector on the illuminating lens system. The HAADF images were recorded with an illumination semiangle of 26.5 mrad, a condition that, with proper correction of several aberration parameters, has routinely provided resolution at the sub-Ångström level. X-ray photoelectron spectroscopy (XPS) data were collected using a PHI 3056 spectrometer with an Al anode source operated at 15 kV and an applied power of 350 W. Samples were manually pressed between two pieces of indium foil; the piece of In foil with the sample on it was then mounted to the sample holder with a piece of carbon tape (Nisshin E.M. Co. LTD). The Si 2p (103.75 eV) and 01s (532.8 eV) lines were used to calibrate the binding energies because the 500 °C annealed sample had no surface carbon. High-resolution data were collected at a pass energy of 5.85 eV with 0.05 eV step sizes and a minimum of 200 scans to improve the signal-to-noise ratio; lower resolution survey scans were collected at a pass energy of 93.5 eV with 0.5 eV step sizes and a minimum of 25 scans.

Catalytic Experiments. To study the catalysts for ethanol oxidation, 50 mg of AuCu nanoparticles supported on SiO_2 was packed into a U-shaped quartz tube (4 mm i.d.) on an Altamira AMI 200 microreactor. The catalysts were pretreated at 300–500 °C for 1 h in 10% O_2/He or at 400 °C in 10% O_2/He, followed by 300 °C in 10% H_2/Ar for 1 h. The catalysts were then cooled to room temperature in 10% O_2/He. During the reaction, 10% O_2/He was bubbled through a saturator maintained at 25 °C containing anhydrous ethanol at a rate of 5 cm^3 min^{-1}, thus producing an ethanol/O_2 reactant mixture of 0.61:1. The temperature of the catalysts was controlled by a furnace and monitored by an internal thermocouple. A portion of the product stream was extracted periodically with an automatic sample valve and analyzed by a GC using a RC-Q-Bond column (30 m, 0.53 mm i.d.) with both a thermal conductivity detector and a flame ionization detector.

RESULTS

Silica-supported AuCu alloy nanoparticle catalysts were prepared in a manner similar to that reported previously. Briefly, premade silica-supported Au catalysts were first added to a $Cu(C_2H_3O_2)_2$ solution of 1-octadecene, oleic acid, and oleylamine and reacted at 300 °C. During the reaction process, the Cu^{2+} ions are reduced to Cu(0) and diffuse into the Au/SiO_2 at elevated temperatures under an inert atmosphere.[12] The face-centered cubic (fcc) structure of Au/SiO_2 is shown in the XRD pattern in the bottom of Figure 1a, with the most

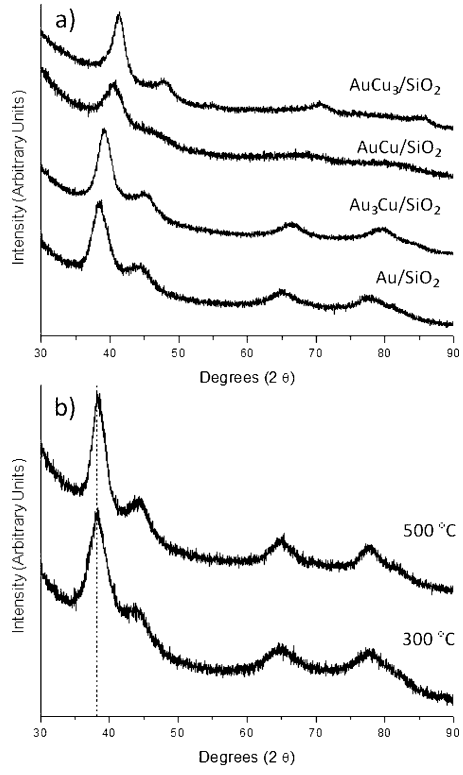

Figure 1. Powder X-ray diffraction pattern of (a) as-synthesized silica-supported Au, Au_3Cu, AuCu, and $AuCu_3$ and (b) $AuCu/SiO_2$ after calcination at 300 and 500 °C in 10% O_2/He for 1 h. The solid vertical line is in reference to the (111) peak position of pure Au.

dx.doi.org/10.1021/cs300551r | ACS Catal. 2012, 2, 2537–2546

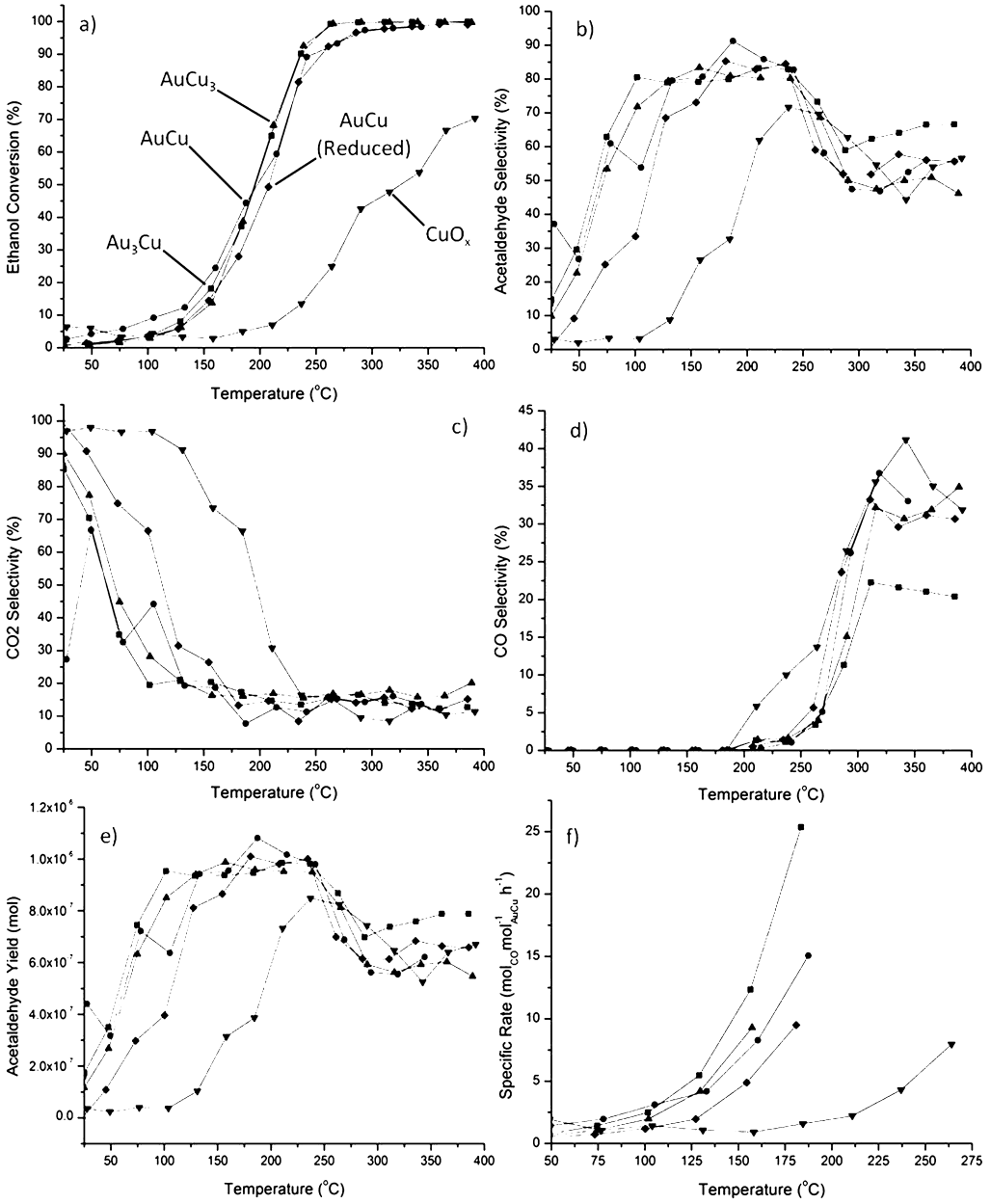

Figure 2. Temperature-dependent ethanol oxidation reaction after 300 °C calcination showing (a) ethanol conversion, (b) acetaldehyde selectivity, (c) CO_2 selectivity, (d) CO selectivity, (e) acetaldehyde molar yield, and (f) specific activity of each catalyst. (♦) $AuCu/SiO_2$ calcined at 300 °C followed by reduction under 10% H_2/Ar at 300 °C and (■) Au_3Cu/SiO_2, (●) $AuCu/SiO_2$, (▲) $AuCu_3/SiO_2$, and (▼) CuO_x/SiO_2 calcined at 300 °C.

intense peak (111) located at 2θ = 38.2. When Cu diffuses into the Au particles, the fcc structure remains, but the Au lattice contracts, and the XRD peaks shift to the right, as seen in the upper three XRD patterns in Figure 1a. Analysis of the AuCu alloys' (111) peak positions at 2θ = 39.1, 40.2, and 41.4 using Vegard's law estimates their compositions to be 64% Cu, 36% Au; 49% Cu, 51% Au; and 19% Cu, 81% Au, respectively. ICP analysis found that the composition of each Au−Cu alloy catalyst was 75% Cu and 25% Au, 48.3% Cu and 52.7% Au, and 31% Cu and 69% Au, respectively. The very broad and low-intensity peaks the AuCu alloy indicate that very small and disperse particles are present on the SiO_2 support, even after high-temperature reaction conditions. To form the Au−CuO_x heterostructures, the AuCu alloy catalysts were oxidized at 300 or 500 °C. Figure 1b shows that when the Cu oxidizes, the fcc pattern shifts from the AuCu alloy position (2θ = 40.2°) to the pure Au position (2θ = 38.2°) signifying that all of the copper has left the gold lattice. This observation is in agreement with previous studies that indicated that $AuCu/SiO_2$ alloy catalysts began to oxidize above 150 °C to form Au−CuO_x.[37,38]

To investigate how alloying of Au with Cu and the formation of the Au−CuO_x heterostructure affected the catalytic activity and selectivity compared with Au/SiO_2 and CuO_x/SiO_2, the gas-phase oxidation of ethanol was monitored, and the results are reported in Figures 2 and 3. All catalysts formed acetaldehyde as the main reaction product, with the maximum selectivity just below 200 °C. Other reaction products that were detected were CO, CO_2, acetic acid, and ethyl acetate; however, each of the latter two components formed <1% of the reaction products and are not shown.

All catalysts calcined at 300 °C are shown in Figure 2. As seen in Figure 2a, the three Au−Cu catalysts have a T_{50} value

dx.doi.org/10.1021/cs300551r | ACS Catal. 2012, 2, 2537−2546

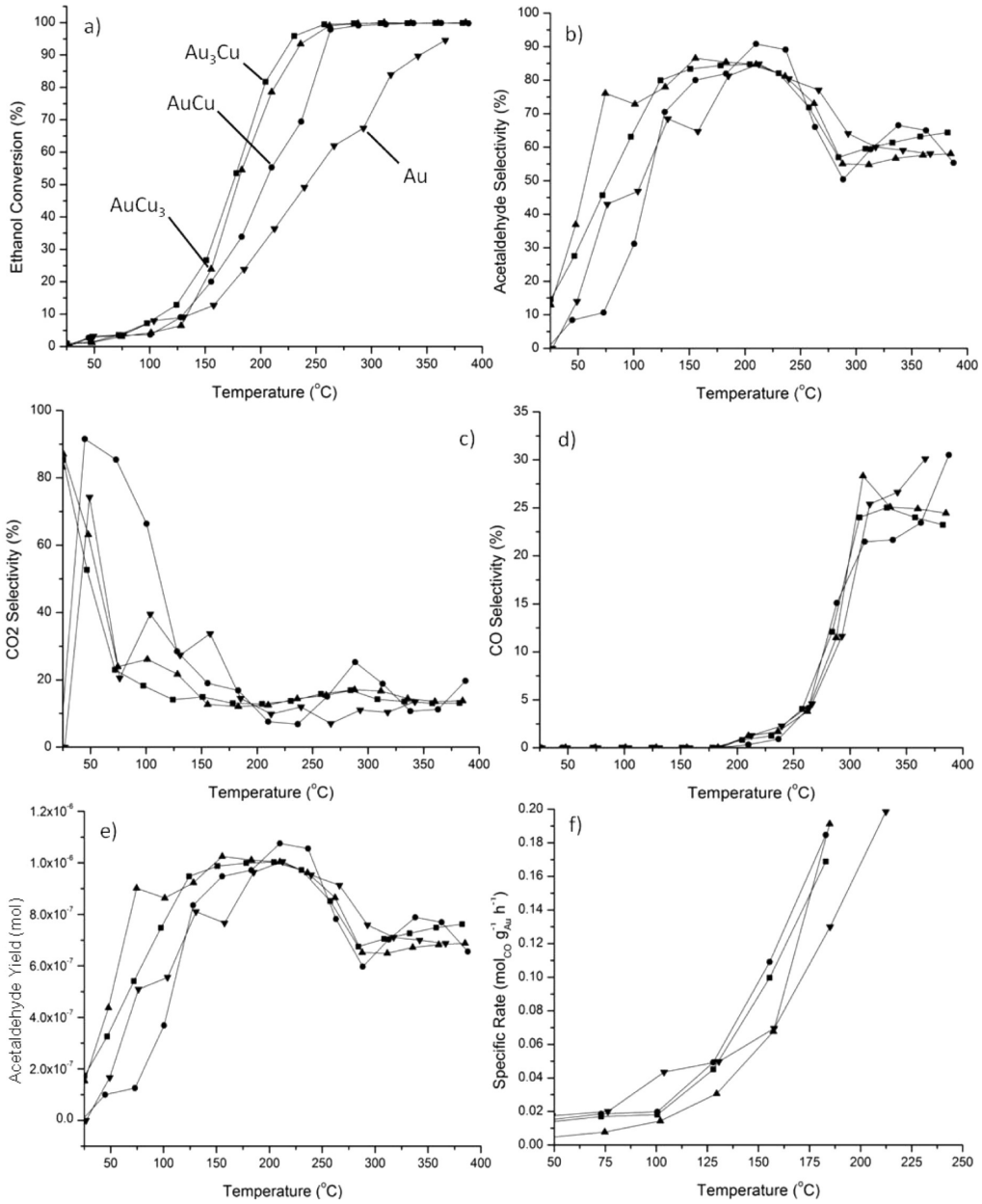

Figure 3. Temperature-dependent ethanol oxidation reaction after 500 °C calcination showing (a) ethanol conversion, (b) acetaldehyde selectivity, (c) CO_2 selectivity, (d) CO selectivity, (e) acetaldehyde molar yield, and (f) specific activity of each catalyst. (■) Au_3Cu/SiO_2, (●) $AuCu/SiO_2$, (▲) $AuCu_3/SiO_2$, and (▼) Au/SiO_2.

for ethanol conversion ~125 °C lower than the CuO_x catalyst. Furthermore, the Au−Cu catalysts were significantly more selective for the formation of acetaldehyde, as seen in Figure 2b and e, at lower temperatures (~80%, 100−150 °C), as compared with CuO_x. Figure 2c and d indicate that CuO_x/SiO_2 prefers the combustion of ethanol and forms a significantly larger amount of CO_2 and CO. To gain a more quantitative comparison between the catalysts, specific rates (mol_{CO} mol_{AuCu}^{-1} h^{-1}) were calculated, in Figure 2f, to normalize the conversion of ethanol to moles of the active metal (Au and Cu) per hour on the basis of ethanol concentration (mol %), flow rate (5 mL/min), ethanol conversion (below 40%), gold loading (based off ICP analysis), and amount of catalyst added to the reactor (50.0−50.3 mg). It is apparent from Figure 2f that the silica-supported Au−Cu catalysts show a higher rate of ethanol conversion at lower temperatures than the CuO_x/SiO_2 catalysts that require temperatures over 200 °C to obtain similar activities. However, it appears that the gold-rich alloy ($Au_{69}Cu_{31}$) composition is the most efficient, as compared with AuCu and $AuCu_3$, because a thicker CuO_x shell may hinder access to the Au active sites. Similar observations were observed in $Au@Fe_2O_3$ core@shell nanoparticles for the oxidation of CO.[43] The reduced $AuCu/SiO_2$ sample also showed activity similar to that of the Au−CuO_x catalysts (calcined at 300 or 500 °C). From previous studies,[37] it is known that the AuCu alloy is resistant to oxidation up to ~150 °C in air before it starts to phase-segregate into Au−CuO_x. Ethanol conversion is observed for the reduced AuCu (alloy) catalyst below 150 °C and suggests that the alloy itself may have some catalytic activity; however, by the time 100% conversion is reached, the Au−CuO_x structure is already formed.

When the catalysts were calcined at 500 °C in 10% O_2 for 1 h, the Au−Cu catalysts produced higher ethanol conversions

dx.doi.org/10.1021/cs300551r | ACS Catal. 2012, 2, 2537−2546

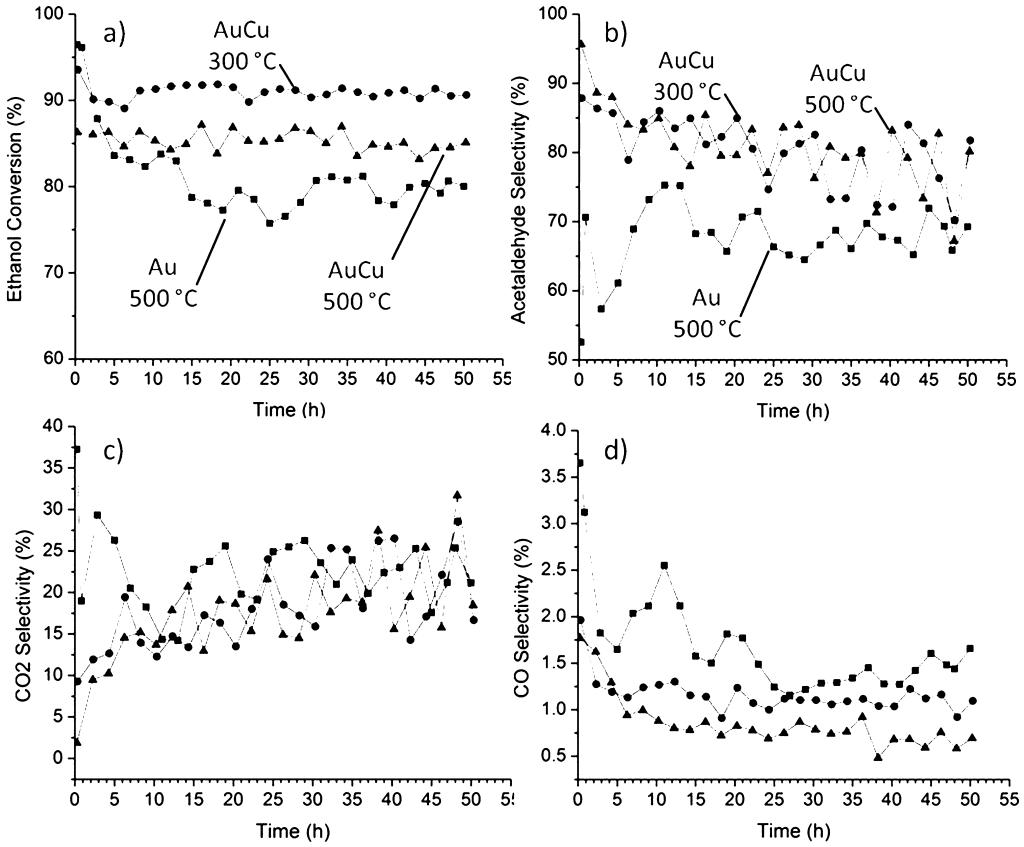

Figure 4. Time-dependent ethanol oxidation at a reaction temperature of 200 °C for 50 h showing (a) ethanol conversion, (b) acetaldehyde selectivity, (c) CO selectivity, (d) CO_2 over (■) Au/SiO_2 calcined at 500 °C, (●) $AuCu/SiO_2$ calcined at 300 °C, and (▲) $AuCu/SiO_2$ calcined at 500 °C.

and were more selective toward acetaldehyde than Au/SiO_2, as seen in Figure 3a, b, and c. In fact, the pure gold catalyst never reached 100% conversion. Figure 3c and d also shows that all catalysts were equally selective in the formation of CO_2 and CO. The specific rates calculated in Figure 2f indicate that, again, the gold rich alloy ($Au_{69}Cu_{31}$) is the most active catalyst, followed by AuCu. The Cu-rich alloy ($Au_{25}Cu_{75}$) showed an ethanol conversion rate similar to gold at the lower temperatures, but the Au−Cu catalysts quickly outperformed Au. As seen earlier, the $AuCu_3$ catalyst is less active, which may be attributed to the thicker CuO_x shell, hindering access to the active sites on Au. These results indicate that when the AuCu alloy particles are oxidized, the Au and CuO_x interfaces are in very close contact, and it is likely that a strong metal−metal oxide interaction exists between the Au and CuO_x. Similar types of Au nanoparticle heterostructures, such as $Au-Fe_3O_4$ dumbbells[30,44] and Au−NiO nanoparticles,[34,35] have also shown an enhancement in the oxidation of CO and parallel the observations in this work. Similarly, a variety of Pd alloys, including Pd−In, Pd−Ga, and Pd−Zn, were found to be more selective for the dehydrogenation of ethanol to form acetaldehyde at the cost of lower conversion.[45] In comparison with other alloy catalysts, Alcala found that alloying Sn with Pt suppressed the decomposition of ethanol to CO, CH_4, and C_2H_6 but favored the dehydrogenation pathway to form acetaldehyde.[46]

To investigate the stability of the $Au-CuO_x/SiO_2$ heterostructured catalysts for the oxidation of ethanol, the samples were run on stream at a constant temperature of 200 °C for 50 h after being subjected to different calcination temperatures; the results of these runs are shown in Figure 4. $AuCu/SiO_2$ was found to be the most active when it was calcined at 300 °C for 1 h in 10% O_2/He and maintained an ethanol conversion at ∼90−93% over a 50 h reaction time. Calcination of the $AuCu/SiO_2$ catalyst at 500 °C showed slightly less catalytic activity, with ∼85% conversion over the same time frame. The silica-supported Au catalyst calcined at 500 °C initially showed the highest conversion in the first 4 h, but steadily declined to between 75 and 80% with large fluctuations in ethanol conversion during the reaction time. The most likely cause for the drop in ethanol conversion with the Au/SiO_2 catalysts in the first 15 h may be particle sintering.

Several studies have shown that the weak interaction between Au and SiO_2 generally produces large particles with low catalytic activity.[47−52] When the $AuCu/SiO_2$ catalyst is calcined at 300 or 500 °C, a $Au-CuO_x/SiO_2$ heterostructure is formed. Figure 5a shows a HAADF image of a typical AuCu alloy particle in which the Au and Cu atoms are homogeneously distributed throughout the nanocrystal. After oxidation at 500 °C in air for 1 h, a thin CuO_x shell, indicated by the less intense contrast layer, formed around the Au particle to create a core−shell structure, as seen in Figure 5b. As shown in Figure 4, when the $Au-CuO_x$ (core−shell structure) is formed, little to no deactivation is observed, and the catalyst remains stable for over a 50 h period. It is likely that CuO_x has a stronger interaction with silica than Au, which can anchor particles to the support, keeping the particles in an optimal size range to efficiently catalyze the reaction. It is also possible that the interface between CuO_x and Au may influence the catalytic properties of Au, as well. As in the case for CO oxidation, Liu

dx.doi.org/10.1021/cs300551r | ACS Catal. 2012, 2, 2537−2546

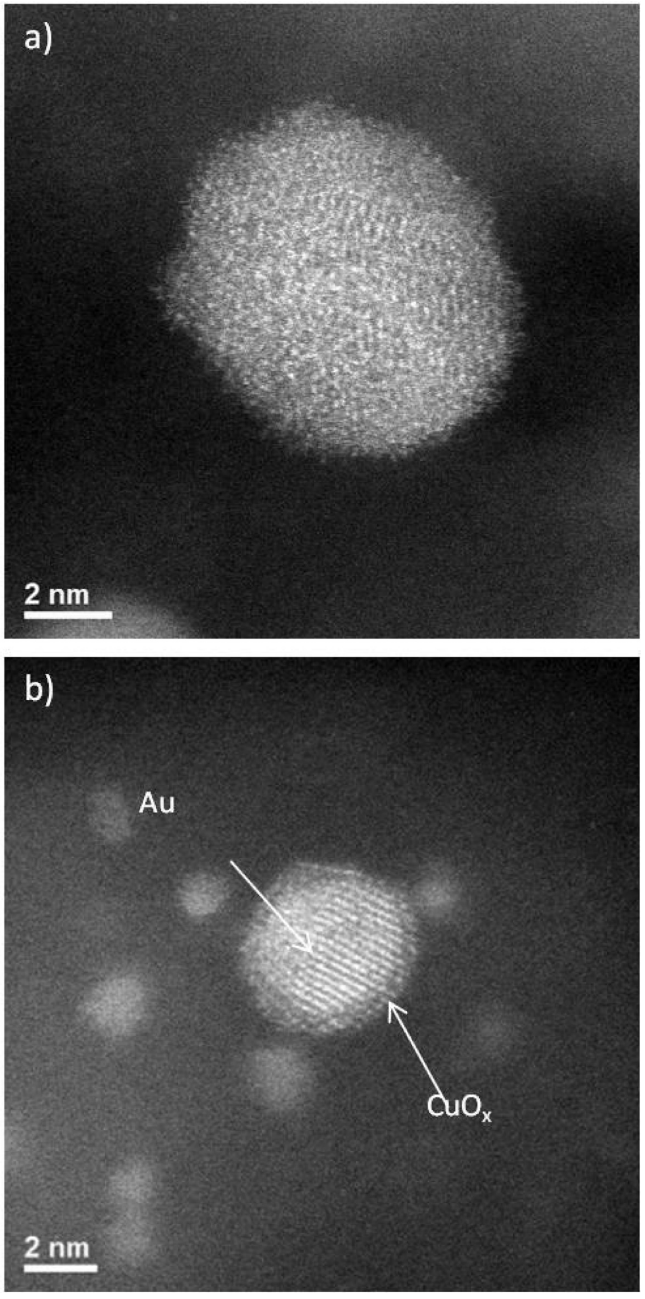

Figure 5. HAADF images of (a) AuCu alloy nanoparticles supported on silica and (b) Au−CuO_x nanoparticles supported on silica after calcination at 500 °C.

and Li have speculated that CuO_x may donate O to the CO that is adsorbed onto the Au particle's surface,[38,39] and this effect may contribute to the improved ethanol oxidation performance of the Au−Cu catalysts.

The CuO_x−Au interface also appears to influence the selectivity of the ethanol oxidation toward acetaldehyde. The Au/SiO_2 catalyst was ~70% selective toward acetaldehyde, which is due not only to slightly higher levels of CO_2 and CO, as can be seen in Figure 4c and d, but also to an increased amount of ethyl acetate formation of ~7% (not shown). A Au/SiO_2 catalyst prepared through a colloidal deposition method with varying particle sizes was reported to show a conversion of no more than 40% of ethanol, with a similar acetaldehyde selectivity under similar reaction conditions.[26] The $AuCu/SiO_2$ catalysts calcined at 300 and 500 °C showed a selectivity of acetaldehyde formation that began in the upper 80% range and gradually decreased to the lower 80% to upper 70% range with increasing fluctuations.

As can be seen from the catalytic results, the combination of pretreatment conditions and time on-stream can influence the catalytic activity and selectivity. Furthermore, previous studies of Au−Cu alloy nanoparticles supported on SiO_2 revealed that oxidizing the system to form Au−CuO_x improved the stability and reduced particle sintering, even after calcination at high temperatures.[37,38,53] The resistance to particle sintering and the stability of the catalyst was examined by TEM after the catalysts (in Figure 4) were subjected to calcination pretreatments and 50 h on-stream at 200 °C. Figure 6a and 6b shows TEM images

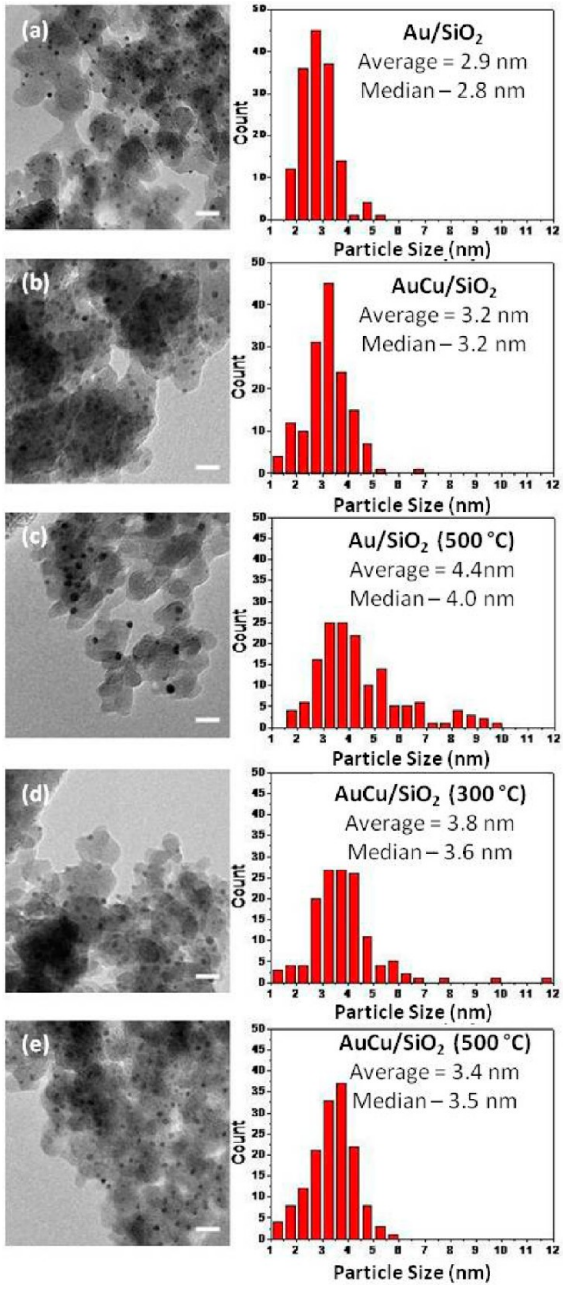

Figure 6. TEM images with their corresponding histograms showing the average nanoparticle diameter for as-synthesized (a) Au/SiO_2 and (b) $AuCu/SiO_2$ as well as the average particle diameter after 50 h of ethanol conversion on-stream at 200 °C for (c) Au/SiO_2, 500 °C calcination; (d) $AuCu/SiO_2$, 300 °C calcination; and (e) $AuCu/SiO_2$, 500 °C calcination.

dx.doi.org/10.1021/cs300551r | ACS Catal. 2012, 2, 2537−2546

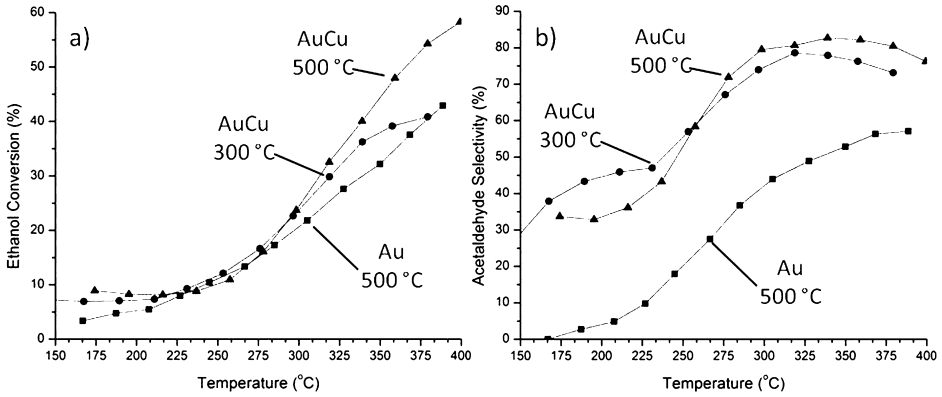

Figure 7. Temperature-dependent ethanol dehydrogenation reaction showing (a) ethanol conversion and (b) acetaldehyde selectivity over (■) Au/SiO_2 calcined at 500 °C, (●) $AuCu/SiO_2$ calcined at 300 °C, and (▲) $AuCu/SiO_2$ calcined at 500 °C.

of as-synthesized Au/SiO_2 (after reduction in H_2 at 150 °C) and $AuCu/SiO_2$, respectively, with their corresponding size distribution histograms. The average size of the silica-supported Au particles was 2.9 nm in diameter, but after undergoing calcination at 500 °C and 50 h reaction time at 200 °C, the particle diameters increased 1.5 times to 4.4 nm.

In addition to the increased particle size of the Au/SiO_2 catalyst, the size distribution is very wide and may be partly responsible for the gradual decrease in ethanol conversion over the 50 h reaction time. In the case of the $Au-CuO_x$ catalysts, a small increase in the particle diameter from 3.2 to 3.8 nm and 3.4 nm was observed after calcination at 300 and 500 °C, respectively. We believe that the reduced particle growth is attributed to the formation of CuO_x that anchors the Au to the silica support and, as seen by TEM, the $Au-CuO_x$ particles are more resistant to particle growth and can maintain high particle dispersion.

The dehydrogenation of ethanol over Au/SiO_2 and $Au-Cu/SiO_2$ catalysts in the absence of oxygen (He atmosphere) was investigated at a temperature range between 165 and 400 °C. Figure 7a shows the ethanol conversion over Au/SiO_2 calcined at 500 °C and $Au-CuO_x/SiO_2$ calcined at 300 and 500 °C in 10% O_2/He. As expected, all three catalysts exhibit a lower catalytic activity in the absence of O_2 and yield acetaldehyde, CO, and CO_2 as the main reaction products. However, both $Au-CuO_x$ samples (calcined at 300 and 500 °C) produce higher ethanol conversion than Au and are nearly twice as selective for acetaldehyde formation. The $Au-CuO_x/SiO_2$ catalyst calcined at 500 °C was the most active; followed by $Au-CuO_x/SiO_2$ calcined at 300 °C; and then, finally, Au/SiO_2 calcined at 500 °C. Interestingly, the $Au-CuO_x$ sample calcined at 300 °C, which maintained the highest ethanol conversion in oxygen at 200 °C, eventually fell in line, with a conversion rate similar to that of Au/SiO_2.

It appears that the CuO_x-Au interface that forms from a higher calcination temperature plays a role in the dehydrogenation of ethanol in an oxygen-deficient environment. The $AuCu/SiO_2$ catalyst calcined at 500 °C was analyzed by XPS before and after catalyzing the dehydrogenation of ethanol in a He atmosphere; the Cu $2p^{3/2}$ XPS data are shown in Figure 8a. The used catalysts were stored in air for several days prior to analysis. These data show a Cu^{2+}-like species (933.3 eV) in the 500 °C annealed sample and a shift of 0.9 eV to a more reduced form of Cu after the catalytic reaction (932.4 eV).[54] Interestingly, the 500 °C annealed sample prior to reaction was devoid of adventitious carbon that is typically present on oxide

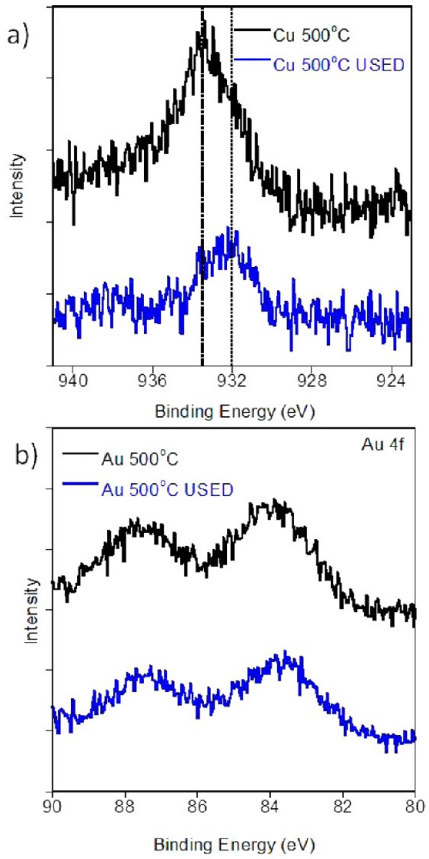

Figure 8. (a) Cu $2p^{3/2}$ and (b) Au 4f XPS data collected for the $AuCu/SiO_2$ catalysts after calcination at 500 °C for 1 h in 10% O_2/He.

surfaces. But on the used catalyst, there was a significant carbon concentration (~7 at. %), which may indicate coke formation during the reaction and is most likely responsible for the decrease in acetaldehyde selectivity above 325 °C. The Au 4f spectra, in Figure 8b, show a single Au species (binding energy 84.0 eV), consistent with metallic gold species. Investigating the anaerobic dehydrogentaion allows us to evaluate the key factors in the reaction pathway.

In the case of a typical metal or metal oxide catalyst, the dehydrogenation of the ethanol begins with the adsorption of hydrogen and an ethoxide species through the cleavage of the O–H bond. FTIR spectra indicate that although ethanol only weakly adsorbs on the silica support, the ethoxide strongly

dx.doi.org/10.1021/cs300551r | ACS Catal. 2012, 2, 2537–2546

binds to the Au nanoparticle surface.[28] Acetaldehyde is then formed through the dehydrogenation of the adsorbed ethoxide. The residual hydrogen left from the ethoxide can then combine with an adsorbed OH or H to form H_2O or H_2, respectively.[40] As has been suggested previously, the presence of oxygen, whether it is in the form of atomic or molecular oxygen, superoxo complexes, or adsorbed OOH species, lowers the activation energy.[55] Under anaerobic conditions, the reaction does not proceed as easily, and it is believed that the β-hydride elimination of the ethoxide is the rate-limiting step. However, the fact that the Au−Cu samples demonstrate superior reactivity and selectivity for both of the aerobic and anaerobic dehydrogenation reactions of ethanol (Figures 2, 3, and 6) indicates that the interface between Au and CuO_x may lower the energy of the rate-limiting step (β-hydride elimination).

The enhancement to the catalytic properties that the Au−CuO_x catalyst offers can be rationalized through examining the hybrid particle's structure. In combination with our own results[37] and other studies,[38] it has been shown that the oxidative dealloying of Au−Cu forms a structure containing a Au core coated by a CuO_x shell, which may consist of CuO islands or a pourus shell. When Au is supported on a reducible oxide support, such as TiO_2, CeO_2, Fe_2O_3, etc., the reducibility of the support is increased at the interface, which increases the mobility of the lattice oxygen to participate in the reaction. The interfacial contact between Au and CuO_x is maximized through the core@shell (or oxide island) structure and results in a highly reducible and active CuO phase that works in synergy with the Au particle. Even in the absence of O_2, the Au−CuO catalyst shows higher ethanol conversions with a higher acetaldehyde selectivity, and XPS results indicate that Cu^{2+} shifts to a more reduced state. It is probable that the close proximity between the CuO phase and the Au metal allows the two materials to work in synergy to convert ethanol into acetaldehyde more efficiently than if they were on their own.

CONCLUSIONS

Au−Cu alloy nanoparticles were synthesized through the diffusion of reduced Cu into silica-supported Au nanoparticles, and these formed Au−CuO_x heterostructures upon oxidation. These heterostructures produced catalysts that are capable of obtaining high selectivity toward acetaldehyde while simultaneously maintaining high conversion for the aerobic and anaerobic dehydrogenation of ethanol. AuCu/SiO_2 catalysts calcined at 300 °C provided the highest ethanol conversion with the highest acetaldehyde formation in the presence of oxygen. However, for the oxidation of ethanol in a He atmosphere, the AuCu catalyst calcined at 500 °C showed the highest conversion of ethanol. When compared with Au/SiO_2 the two calcined AuCu/SiO_2 (300 and 500 °C) samples were found to be more resistant to sintering and showed less than 0.6 nm increase in particle diameter after being subjected to pretreatment and catalytic conditions. It is becoming evident that when metal−oxide interfaces are created through the formation of heterostructures, the catalytic properties appear to change significantly. It is likely that the CuO_x increases the resistance to sintering, thus allowing the particles to remain in an optimal size range to catalyze the oxidation of ethanol. Furthermore, the Au−CuO_x interface and the possible O donation from CuO_x contribute to the enhanced catalytic activity and selectivity toward acetaldehyde formation. We postulate that the interface between the metal and the metal oxide is one of the most active sites of the catalyst, and it is important to increase the contact area of these interfaces to maximize the catalytic activity. Oxidative dealloying of supported alloy nanoparticle catalysts is a valuable method of forming heterostructured catalysts that take advantage of the increased interfacial contact between the metal and the metal oxide to help promote catalytic activity, selectivity, and catalyst stability.

AUTHOR INFORMATION

Corresponding Author

*Phone: (865)574-5033. Fax: (865)576-5235 dais@ornl.gov. E-mail: dais@ornl.gov.

Notes

The authors declare no competing financial interest.

ACKNOWLEDGMENTS

The research was sponsored by the Division of Chemical Sciences, Geosciences, and Biosciences, Office of Basic Energy Sciences, U.S. Department of Energy, under Contract No. DE-AC05-00OR22725 with Oak Ridge National Laboratory managed and operated by UT-Battelle, LLC. A portion of this work (G.M.V.) was supported by the U.S. Department of Energy's Office of Basic Energy Science, Division of Materials Sciences and Engineering, under contract with UT-Battelle, LLC. A portion of this research was conducted at the Center for Nanophase Materials Sciences, which is sponsored at Oak Ridge National Laboratory by the Scientific User Facilities Division, U.S. Department of Energy.

REFERENCES

(1) Rass-Hansen, J.; Falsig, H.; Jørgensen, B.; Christensen, C. H. *J. Chem. Technol. Biotechnol.* **2007**, *82* (4), 329−333.
(2) Jørgensen, B.; Egholm Christiansen, S.; Dahl Thomsen, M. L.; Christensen, C. H. *J. Catal.* **2007**, *251* (2), 332−337.
(3) Mallat, T.; Baiker, A. *Chem. Rev.* **2004**, *104* (6), 3037−3058.
(4) Vogler, T.; Studer, A. *Synthesis (Stuttgart)* **2008**, *13*, 1979−1993.
(5) Vinod, C. P.; Wilson, K.; Lee, A. F. *J. Chem. Technol. Biotechnol.* **2011**, *86* (2), 161−171.
(6) Corma, A.; Garcia, H. *Chem. Soc. Rev.* **2008**, *37* (9), 2096−2126.
(7) Obana, Y.; Uchida, H.; Sano, K.-i., Patent 6,867,164, 2005.
(8) Prati, L.; Rossi, M. In *Proceedings of the 3rd World Congress on Oxidation Catalysis*; San Diego, CA, September 21−26, 1997; Elsevier: New York, Amsterdam; 1997; Vol. *110*; pp 509−516.
(9) Prati, L.; Rossi, M. *J. Catal.* **1998**, *176* (2), 552−560.
(10) Prati, L.; Martra, G. *Gold Bull.* **1999**, *32* (3), 96−101.
(11) Porta, F.; Prati, L.; Rossi, M.; Coluccia, S.; Martra, G. *Catal. Today* **2000**, *61* (1−4), 165−172.
(12) Biella, S.; Rossi, M. *Chem. Commun.* **2003**, *3*, 378−379.
(13) Carrettin, S.; McMorn, P.; Johnston, P.; Griffin, K.; Kiely, C. J.; Hutchings, G. J. *Phys. Chem. Chem. Phys.* **2003**, *5* (6), 1329−1336.
(14) Bianchi, C. L.; Canton, P.; Dimitratos, N.; Porta, F.; Prati, L. *Catal. Today* **2005**, *102−103* (0), 203−212.
(15) Enache, D. I.; Knight, D. W.; Hutchings, G. J. *Catal. Lett.* **2005**, *103* (1), 43−52.
(16) Meenakshisundaram, S.; Nowicka, E.; Miedziak, P. J.; Brett, G. L.; Jenkins, R. L.; Dimitratos, N.; Taylor, S. H.; Knight, D. W.; Bethell, D.; Hutchings, G. J. *Faraday Discuss.* **2010**, *145*, 341−356.
(17) Enache, D. I.; Edwards, J. K.; Landon, P.; Solsona-Espriu, B.; Carley, A. F.; Herzing, A. A.; Watanabe, M.; Kiely, C. J.; Knight, D. W.; Hutchings, G. J. *Science* **2006**, *311* (5759), 362−365.
(18) Dimitratos, N.; Lopez-Sanchez, J. A.; Morgan, D.; Carley, A.; Prati, L.; Hutchings, G. J. *Catal. Today* **2007**, *122* (3−4), 317−324.
(19) Dimitratos, N.; Lopez-Sanchez, J. A.; Anthonykutty, J. M.; Brett, G.; Carley, A. F.; Tiruvalam, R. C.; Herzing, A. A.; Kiely, C. J.; Knight, D. W.; Hutchings, G. J. *Phys. Chem. Chem. Phys.* **2009**, *11* (25), 4952−4961.
(20) Hutchings, G. J. *Dalton Trans.actions* **2008**, (41).

(21) Rass-Hansen, J.; Falsig, H.; Jorgensen, B.; Christensen, C. H. *J. Chem. Technol. Biotechnol.* **2007**, *82*, 329−333.
(22) Christensen, C. H.; Jørgensen, B.; Rass-Hansen, J.; Egeblad, K.; Madsen, R.; Klitgaard, S. K.; Hansen, S. M.; Hansen, M. R.; Andersen, H. C.; Riisager, A. *Angew. Chem., Int. Ed.* **2006**, *45* (28), 4648−4651.
(23) Tembe, S.; Patrick, G.; Scurrell, M. *Gold Bull.* **2009**, *42* (4), 321−327.
(24) Sun, K.-Q.; Luo, S.-W.; Xu, N.; Xu, B.-Q. *Catal. Lett.* **2008**, *124* (3), 238−242.
(25) Zheng, N.; Stucky, G. D. *Chem. Commun.* **2007**, *37*, 3862−3864.
(26) Zheng, N.; Stucky, G. D. *J. Am. Chem. Soc.* **2006**, *128* (44), 14278−14280.
(27) Guan, Y.; Hensen, E. J. M. *Appl. Catal., A* **2009**, *361* (1−2), 49−56.
(28) Gazsi, A.; Koós, A.; Bánsági, T.; Solymosi, F. *Catal. Today* **2011**, *160* (1), 70−78.
(29) Simakova, O. A.; Sobolev, V. I.; Koltunov, K. Y.; Campo, B.; Leino, A.-R.; Kordás, K.; Murzin, D. Y. *ChemCatChem* **2010**, *2* (12), 1535−1538.
(30) Wang, C.; Yin, H.; Dai, S.; Sun, S. *Chem. Mater.* **2010**, *22* (10), 3277−3282.
(31) Okumura, M.; Akita, T.; Haruta, M.; Wang, X.; Kajikawa, O.; Okada, O. *Appl. Catal., B* **2003**, *41* (1−2), 43−52.
(32) Akita, T.; Okumura, M.; Tanaka, K.; Tsubota, S.; Haruta, M. *J. Electron Microsc.* **2003**, *52* (2), 119−124.
(33) Liu, Z.-P.; Jenkins, S. J.; King, D. A. *Phys. Rev. Lett.* **2004**, *93* (15), 156102.
(34) Zhou, S.; Ma, Z.; Yin, H.; Wu, Z.; Eichhorn, B.; Overbury, S. H.; Dai, S. *J. Phys. Chem. C* **2009**, *113* (14), 5758−5765.
(35) Zhou, S.; Yin, H.; Schwartz, V.; Wu, Z.; Mullins, D.; Eichhorn, B.; Overbury, S. H.; Dai, S. *ChemPhysChem* **2008**, *9* (17), 2475−2479.
(36) Yu, K.; Wu, Z.; Zhao, Q.; Li, B.; Xie, Y. *J. Phys. Chem. C* **2008**, *112* (7), 2244−2247.
(37) Bauer, J. C.; Mullins, D.; Li, M.; Wu, Z.; Payzant, E. A.; Overbury, S. H.; Dai, S. *Phys. Chem. Chem. Phys.* **2011**, *13* (7), 2571−2581.
(38) Liu, X.; Wang, A.; Li, L.; Zhang, T.; Mou, C.-Y.; Lee, J.-F. *J. Catal.* **2011**, *278* (2), 288−296.
(39) Li, X.; Fang, S. S. S.; Teo, J.; Foo, Y. L.; Borgna, A.; Lin, M.; Zhong, Z. *ACS Catal.* **2012**, *2*, 360−369.
(40) Idriss, H.; Seebauer, E. G. *J. Mol. Catal A: Chem.* **2000**, *152* (1−2), 201−212.
(41) Zhu, H. G.; Ma, Z.; Clark, J. C.; Pan, Z. W.; Overbury, S. H.; Dai, S. *Appl. Catal., A* **2007**, *326* (1), 89−99.
(42) Rao, R. S.; Walters, A. B.; Vannice, M. A. *J. Phys. Chem. B* **2004**, *109* (6), 2086−2092.
(43) Yin, H.; Ma, Z.; Chi, M.; Dai, S. *Catal. Today* **2011**, *160* (1), 87−95.
(44) Yin, H.; Wang, C.; Zhu, H.; Overbury, S. H.; Sun, S.; Dai, S. *Chem. Commun.* **2008**, *36*, 4357−4359.
(45) Iwasa, N.; Yamamoto, O.; Tamura, R.; Nishikubo, M.; Takezawa, N. *Catal. Lett.* **1999**, *62* (2), 179−184.
(46) Alcala, R.; Shabaker, J. W.; Huber, G. W.; Sanchez-Castillo, M. A.; Dumesic, J. A. *J. Phys. Chem. B* **2004**, *109* (6), 2074−2085.
(47) Chi, Y. S.; Lin, H. P.; Mou, C. Y. *Appl. Catal., A* **2005**, *284* (1−2), 199−206.
(48) Yang, C. M.; Kalwei, M.; Schuth, F.; Chao, K. J. *Appl. Catal., A* **2003**, *254* (2), 289−296.
(49) Overbury, S. H.; Ortiz-Soto, L.; Zhu, H. G.; Lee, B.; Amiridis, M. D.; Dai, S. *Catal. Lett.* **2004**, *95* (3−4), 99−106.
(50) Guczi, L.; Peto, G.; Beck, A.; Frey, K.; Geszti, O.; Molnar, G.; Daroczi, C. *J. Am. Chem. Soc.* **2003**, *125* (14), 4332−4337.
(51) Martra, G.; Prati, L.; Manfredotti, C.; Biella, S.; Rossi, M.; Coluccia, S. *J. Phys. Chem. B* **2003**, *107* (23), 5453−5459.
(52) Okumura, M.; Haruta, M. *Chem. Lett.* **2000**, *4*, 396−397.
(53) Liu, X. Y.; Wang, A. Q.; Wang, X. D.; Mou, C. Y.; Zhang, T. *Chem. Commun.* **2008**, *27*, 3187−3189.
(54) Panzner, G.; Egert, B.; Schmidt, H. P. *Surf. Sci.* **1985**, *151* (2−3), 400−408.
(55) Guan, Y.; Hensen, E. J. M. *Appl. Catal., A* **2009**, *361* (1−2), 49−56.